Wang Jie (Orcid ID: 0000-0003-4904-2394)

Dai Zhijun (Orcid ID: 0000-0001-7682-0310)

Fagherazzi Sergio (Orcid ID: 0000-0002-4048-5968)

Tropical cyclones significantly alleviate mega-deltaic erosion induced by high riverine flow

Jie Wang[1,3], Zhijun Dai[1,2*], Xuefei Mei[1], Sergio Fagherazzi[3]

[1]State Key Laboratory of Estuarine and Coastal Research, East China Normal University, Shanghai, China

[2]Laboratory for Marine Geology, Qingdao National Laboratory for Marine Science and Technology, Qingdao, China

[3]Department of Earth and Environment, Boston University, Boston, USA

[*]Corresponding author:

Zhijun Dai

State Key Laboratory of Estuarine and Coastal Research, East China Normal University, Shanghai, China

Email: zjdai@sklec.ecnu.edu.cn

Tel: +86 21 62233458

Fax: +86 21 62546441

This article has been accepted for publication and undergone full peer review but has not been through the copyediting, typesetting, pagination and proofreading process which may lead to differences between this version and the Version of Record. Please cite this article as doi: 10.1029/2020GL089065

Key Points

1. High riverine flow during the flood season triggers massive erosion in the Changjiang Delta.
2. Tropical cyclones reduce the overall fluvial erosion during the flood season.
3. Deposition triggered by typhoons can offset 50% of the estuarine erosion caused by high riverine flow

Abstract

The drastic decline in sediment discharge experienced by large rivers in recent years might trigger erosion thus increasing the vulnerability of their extensive deltas. However, scarce information is available on the erosion patterns in mega-deltas and associated physical drivers. Here, a series of bathymetries in the South Passage, Changjiang Delta, were analyzed to identify morphodynamic variations during high riverine flow and tropical cyclones (TC). Results indicate that high river flow during flood season triggers large-scale net erosion along the inner estuary, generating elongated erosion-deposition patches. Erosion magnitude gradually weakens moving seaward with few localized bottom variations in the offshore area. TCs transport sediment landward and are accompanied by an overall weak erosion, with a less organized spatial pattern of erosion-deposition. TCs can therefore significantly alleviate erosion, reducing the sediment loss induced by riverine flows by over 50%. These results highlight the role of TCs on the sediment dynamics of mega-deltas.

Plain Language Summary

In recent years, climate change and reduced riverine sediment inputs have significantly affected the morphology of large deltas. However, it is unknown whether typhoons cause erosion or deposition in the submerged part of a delta, due to challenge in capturing infrequent events. Here, we study the impact of high river flow and typhoons on the South Passage, Changjiang Delta. Results show that high riverine flows can cause large-scale erosion. Typhoons reduce fluvial erosion by transporting offshore sediments in the delta. The relative accretion caused by a typhoon is more than half the net erosion induced by riverine floods. This research sheds light on the sediment budget of large deltas and inform policy measures that can mitigate the effect of increasing anthropogenic pressure, extreme events, and sea level rise on delta morphology.

Keywords

Deltaic morphodynamics; Sediment budget of deltas; High runoff; Typhoon events; Changjiang Delta

1. Introduction

Large deltas around the world are shaped by riverine inputs and oceanic forces, which undertake important eco-environmental services like land building and biological habitat construction (Woodroffe et al., 1989; Fagherazzi and Overeem, 2007). Unfortunately, many deltas have been experiencing serious erosion induced by a drastic decline in suspended sediment discharge (SSD) from upstream (Syvitski et al., 2005; Ortiz et al., 2017). Estuarine erosion induced by insufficient SSD could also be aggravated by an increase in the frequency of tropical cyclones (TCs) triggered by global warming (Filgueira et al., 2014; Masselink et al., 2016). Recently, the impact of upstream dams on delta morphodynamics has received global attention, but few studies have explored the geomorphic response of deltas to large tropical storms, due to the challenge in collecting detailed bathymetries pre- and post-storm events (Gracia et al., 2019).

Energetic TCs can generate significant changes in estuarine-deltaic morphology. In 2005, Hurricanes Cindy, Katrina, and Rita eroded 9.1×10^6 m^3 of sediment from a 47.9 km^2 area of the Mississippi delta, USA, and accounted for 63% of the total erosion in the distal ebb-tidal region (Miner et al., 2009). However, Hurricane Sandy only caused minor estuarine morphological change in Barnegat Inlet, New Jersey, and induced a sediment deposition of 3 cm across the near shore and inner shelf of the Mid-Atlantic Bight (Miles et al., 2015; Miselis et al., 2016). Therefore, whether erosion or deposition occurs during TCs is still undetermined, particularly in mega deltas experiencing a reduction in riverine sediment inputs.

The Changjiang Delta (Figure 1a-1b) is frequently impacted by periodic East Asian Monsoons. Large amounts of riverine water and SSD are discharged in the funnel-shaped estuary during the monsoon season, developing bifurcations with migrating channels and tidal bars. Some studies indicate that the fluvial SSD input has decreased by 70% after the construction of the Three Gorges Dam (TGD) in 2003, triggering local erosion in the offshore area of the Changjiang delta (Dai et al., 2016; Wang et al., 2018). Recent studies suggest that sediment supplied from the ocean can alleviate the current estuarine erosion, providing material to tidal flats and shoals (Dai et al., 2013 & 2018; Yang et al., 2017). However, it is still debatable whether different deltaic areas are eroding or depositing during and after TCs. Previous work

suggests that summer typhoons cause large-scale erosion in the Changjiang deltaic front (Yang et al., 2003; Hu et al., 2009; Zhang et al., 2018), while winter storms evacuate alluvial sediments deposited in the northern part of Changjiang Delta and transfer the eroded material to deeper channels (Wan et al., 2014). Extreme storms and river floods might also cause large-scale erosion and deposition in the subaqueous delta (Dai et al., 2014), but for the inner part of the Changjiang estuary such a study has not been carried out.

Here we select the South Passage (SP) (Figure 1b) to study how Typhoon Ampil, which landed during the flood season in July 2018, affected the estuarine and offshore bathymetry. The SP is the main venue for water and sediment transport in the Changjiang Delta (Text S1). Owing to a reduction in sediment inputs after the TGD impoundment, the natural deltaic evolution has been affected by large erosion (Dai et al., 2015) (Figure S1 and Table S1). During the flood season huge amounts of fluvial sediments are transported to the outer part of the delta. In the dry season, the sediments accumulated offshore are transferred back to the SP by tidal currents (Yun, 2004; Chen et al., 2006). In particular, during extreme runoff events, shoals are eroded by shifting distributaries, changing the morphology of the delta (Yun, 2004; Mei et al., 2018; Wei et al., 2019).

The main objectives of this paper are to: (1) measure morphodynamic variations induced by the Changjiang high flow during the flood season. (2) identify morphodynamic changes generated by a typhoon event. (3) compare the contributions of high riverine flow and typhoons to the sediment budget and morphology of the Changjiang Delta. Our results can enhance the understanding of geomorphic processes caused by extreme events, and reassess the role of different drivers in the long-term evolution of the delta, thus providing important information for the management and sustainability of these environments.

2. Data acquisition and analysis

2.1 Typhoon Ampil

Typhoon Ampil was the third tropical cyclone directly landing in the Changjiang Delta over the past seventy years. It formed in the Western Pacific Ocean east of Luzon Island on July 17, 2018, then gradually strengthened and moved northwestward maintaining its peak

strength. Ampil landed in Chongming Island, Shanghai, on July 22 2018 at 12:30 p.m. (Figure 1b). The Ampil track almost coincided with the channel axis of the SP. The maximum wind speed at Okinawa Island was 31.4 m/s and increased to 33.1 m/s at JiguJiao, offshore of the Changjiang Delta (Figure 1b-1c). At an adjacent ground meteorological station in Sanjiagang, terrestrial wind speed measured about 5 m above local mean sea level sharply increased on July 22 from 4.1 m/s to nearly 9.0 m/s at 7:00 a.m. and did not decrease until 23:00 p.m. (Figure 1d).

2.2 Data acquisition

We systematically collected 4 datasets to analyze delta morphodynamics. The first dataset includes a total of 12 biannual bathymetries from 2000 to 2018 (Table S2) and nautical-charts in 1979 and 2000. This dataset was used to reveal bottom variations and erosion-deposition patterns. Data collected in February or May refer to normal hydrological conditions, while data collected in August represent the impact of high riverine flow during the flood season or during an occasional typhoon event. Ancillary data indicate that 2011, 2013 and 2016 were high flow years, while in 2000 and 2015 Typhoon Kai-tak and Chan-hom landed near the delta (Figure S2). The second dataset encompasses specific parameters of typhoons landed in 2000, 2015, and 2018, including tracks, timing, central pressures and wind speeds (Figure 1c and S2, Table S3). These data were provided by the Chinese Central Meteorological Administration (Figure 1d). A third group of data includes monthly discharge and SSD of the Changjiang river at the Datong station between 2000 and 2018. Data were acquired by the Changjiang Water Resources Commission. Finally, multiple Landsat images were used to explore estuarine flow-sediment transport patterns under normal, high flow, and typhoon conditions (Table S4).

2.3 Methods

Bathymetric variations from May to August in the SP in the absence of typhoon events were used to quantify the effect of large river discharge on delta morphology. In years when a typhoon landed, bathymetric variations from May to August characterize the combined impact of typhoons and high-water discharge on delta morphology. An ArcGIS 10.1 analysis of bathymetric data determined geomorphic features and variations in sediment volumes (Text S2

and S3). To this end, SP was divided in two sub-regions: i) the inner estuary; ii) the offshore area. The inner estuary includes the main channel and it is relatively sheltered from waves. This area is mostly affected by fluvial discharge and SSD. The offshore area in front of the mouth bars is dominated by tidal currents and wind waves (Figure 1b).

The one-dimensional Fast Fourier Transforms (1D-FFT) were utilized to quantify the spatial periodic characteristics of bathymetric changes (Kroon et al., 2008) (Figure 1e and Text S3). A high spectral energy indicates rhythmic bathymetric changes, typical or migrating bars or shifts in channel thalweg. The Shannon's Diversity Index (SHDI) was adopted to compare bathymetric changes driven by erosion or deposition (Castagno et. al, 2006) (Text S3).

3. Results

3.1 Morphodynamic variations in the absence of typhoons

3.1.1 Patterns of erosion and deposition

Large-scale erosion occurred along the entire SP during the flood season of 2016, in the absence of typhoons (Figure 2a). The inner estuary was characterized by severe scour with elongated areas of erosion alternated with elongated areas of accretion (Figure 2a). Weak erosion with some scattered depositional patches characterized the offshore area (Figure 2a). Few areas with substantial scour were detected at the margin of the Jiuduansha shoal. Erosion magnitude was larger in the inner estuary and decreased toward the offshore area. The eroded area covered 465.0 km^2, corresponding to 74.7% of the total area; the deposition area was 157.9 km^2, and the net eroded volume was up to 64.5×10^6 m^3 (Table S5). In 2016, the volume eroded in the offshore area was only 25.0% of the volume eroded in the inner estuary, while the average elevation change was only 27.8% of the change experienced in the inner estuary (Table S5).

Frequency histograms show that the erosion magnitude mainly ranged between -0.15 to 0 m in 2016; the area affected by these erosion rates covered 42.3% of the total area (Figure 2b). The SHDI of bathymetric variations for the entire SP was 2.0, which indicates that erosion occurred at all scales of magnitude (Table S6). The SHDI in the inner estuary (2.3) was larger than that in the offshore area (1.4), suggesting that the upstream morphological change displayed a larger range of variations probably due to coherent erosion structures affecting the

main tidal channel, while downstream the erosion was more uniform (Table S6, Figure 2a). The total spectral energy of each transverse section computed with the 1D FFT gradually diminished moving offshore, with six peaks in the inner estuary caused by the elongated erosion and deposition zones (Figure 2c).

Similar large-scale scouring also took place during the flood seasons of previous years in the absence of typhoons (in 2011 and 2013, Figure S3a-S3b). Although the total net erosion in these years was similar to 2016 (eroded volumes of 54.5×10^6 m^3 in 2011 and 29.8×10^6 m^3 in 2013) (Table S5), the upstream erosion was relatively lower (Figure 2a and S3a-S3b). The longitudinal patches of erosion and deposition were consistent with those observed in 2016, and mainly developed in the middle of the inner estuary and on the northwest side of the offshore area (Figure S3a-S3b). In 2011, the total spectral energy of bathymetric change decreased less in the downstream direction, and the spectral peaks were smaller and located slightly upstream (Figure S3c). In 2013, the spectral peaks increased significantly of about 3-5 times with respect to 2011.

3.1.2 Estuarine bathymetric changes

Mean bathymetric changes were different within different elevation intervals (Figure 2d). In the flood season of 2016, the high flow caused significant erosion in tidal flats shallower than -3 m bordering the mainland, where the mean erosion exceeded 27.6 cm (Figure 2d). The erosion magnitude within the subtidal zone and in medium-depth channels (between the -3 m and -8 m) was relatively moderate, with a mean value of 8.6 cm and a small standard deviation (Figure 2d). On the contrary, the erosion in channels deeper than -8 m increased to 13.7 cm. Bathymetric variations after the flood seasons in 2011 and 2013 had similar distributions, except for net deposition occurring in 2013 in the shallow Nanhui tidal flats (Figure S4). Longitudinal changes in thalweg elevation are presented in Figure 2e. in 2016 the thalweg elevation did not change uniformly in the inner estuary, with erosion up to 0.8 m is some areas and deposition of 0.4 m in others; fluctuations were present also downstream with deposition near the mouth bar at km 37. Seaward of this location, the elevation change was relatively small, especially in areas deeper than -8 m (Figure 2e).

3.2 Changes in estuarine bathymetry after typhoons

3.2.1 Patterns of erosion and deposition

Typhoon Ampil in 2018 caused distinct changes in bathymetry, and generated a broad and uniform weak erosion (0.1-0.5 m) in the offshore area close to the storm track (Figure 3a). In the inner estuary, areas of erosion and deposition were scattered and not organized in a spatial structure (Figure 3a). Areas affected by strong erosion after the flood season of 2016 in the middle of the inner estuary and near the Jiuduansha Shoal were replaced by scattered patches of erosion and deposition. Deposition patches covered a surface between 2 and 12 km^2 (Figure 3a). In 2018, erosion was much smaller throughout the SP: the area under erosion was 434.9 km^2 (69.7% of total area), while the area affected by deposition increased to 189.3 km^2 (30.3%), with a net decrease in eroded volume of 33.3×10^6 m^3 (Table S5). Net variations in sediment volume and mean erosion thickness in the offshore area were 2.3 and 2.6 times those in the inner estuary.

Frequency histograms show that erosion magnitude for elevations between -1.0 and -0.2 m decreased in 2018 with respect to 2016, while erosion increased for elevations between -0.2 and 1.0 m (Figure 3b). The SHDI in the inner estuary decreased to 2.1 while it increased to 1.5 in the offshore area (Table S6) These values are consistent with the upstream scattered erosion-deposition patterns triggered by Typhoon Ampil. The SHDI of the entire SP decreased to 1.9 with respect to 2.0 in 2016, which indicates that the random disturbances triggered by the strong typhoon reduced the diversity of bathymetric variations. In 2018 the peaks in cross-sectional spectral energy moved slightly upstream, while the number of secondary peaks increased (Figure 3c).

After Typhoon Kai-tak in 2000, erosion in the inner estuary reached 10.3 cm, but large siltation patches were present between eroded areas (Figure 54a). After Typhoon Chan-hom in 2015, the inner estuary mainly experienced weak erosion similar in magnitude to the effect of Typhoon Ampil in 2018 (Figure S5b). The two typhoons in 2000 and 2015 also significantly affected the cross-sectional spectral energy, with peaks moving upstream, and peak values higher than those after river floods (Figure S5c).

3.2.2 Estuarine bathymetric changes

In 2018, tidal flats bordering the mainland and areas shallower than -3 m were affected by

a mean deposition of 2.1 cm (Figure 3d), while erosion occurred in areas of medium water depth (-3 to -10 m). Deeper channels showed a complex response with both siltation and erosion. During the typhoon seasons of 2000 and 2015, local erosion or deposition did not exceed 20 cm (Figure S6). Changes in thalweg elevation after Ampil show that siltation was around 0.5 m in the upstream part of the inner estuary and near the mouth bars (located at 38-52 km), while the offshore zone was characterized by erosion (Figure 3e).

3.3 Mitigation of deltaic erosion driven by typhoons

In this study, data spanning several years were used to quantitatively estimate how typhoons reduce the erosion induced by high riverine flow during flood season. To this end we use the following formula:

$$p_{typhoon} = (\Delta_{typhoon} - \Delta_{flow})/\Delta_{flow} \quad (1)$$

where $\Delta_{typhoon}$ is net bathymetric change induced by a typhoon event during the flood season, negative/positive values represent net erosion/deposition volumes; Δ_{flow} is net bathymetric change caused by high riverine Changjiang flow in the absence of typhoons, $p_{typhoon}$ is the fraction of erosion/deposition volumes to be ascribed to a typhoon with respect to the volume change triggered by the Changjiang high flow.

Bathymetric changes in 2016 (high riverine flow) and 2018 (typhoon) were compared: Typhoon Ampil reduced erosion by 31.2×10^6 m^3, with $p_{typhoon}$ = -0.484 (48.4%). Overall, Typhoon Ampil appears to have weakened the severe erosion caused by high flood flow in 2016 by 80.7% in the inner estuary, and increased erosion in the offshore area by 81.2%. Similarly, Typhoon Chan-hom in 2015 alleviated the net erosion caused by the high Changjiang flow in 2013, with a total erosion of 17.8×10^6 m^3, equivalent to 59.8% of the erosion in 2013. The reduction was more prominent in the inner estuary (40.1%) than in the offshore area (63.1%). Considering the frequency and intensity of TCs, the yearly total amount of seaward sediment carried upstream by them is about 8.91-46.83×10^6 m^3, which is equivalent to 8%-46% of the terrestrial input after the TGD construction. Therefore, we conclude that typhoons alleviate the net erosion caused by the high Changjiang flow during the flood season. We found a significant relationship between the recovered erosion thickness and the average of the top 30 daily values of river discharge in one year. The recovered thickness grows linearly with

discharge both in the inner estuary and for the entire SP, but decreases linearly in the offshore area (Figure 4a-4c).

4. Discussion

4.1 Impact of high riverine flow

High flow during the flood season typically scours the bottom of estuaries, transporting sediment offshore and triggering net erosion (Figure 4d). These dynamics have been showed to exist in most estuaries as, for instance, in the Gironde Estuary in France, in the Mgeni Estuary in South Africa and in the Ba Lat Estuary in Vietnam (Castaing and Allen, 1981; Cooper 2002; Van Maren and Hoekstra, 2004; Allison et al., 2017). In the Changjiang Delta a large volume of fine SSD is transported seaward under high runoff (Figure S7a-S7c). River runoff is dominant in the inner estuary where the flow is confined. When the flow spreads moving seaward, the erosion gradually weakens and it is sometimes replaced by deposition in the offshore area (Figure 4d). Similar erosion and deposition dynamics as a function of riverine flow occur in the Gironde Estuary, France. Here, during high freshwater flow, the mud deposits are progressively scoured, and then redistributed across the shelf covering an area double of that affected by low flow (Lesourd et al., 2003). However, some studies suggest that only extreme floods, rather than normal high flow during the flood season, can induce estuarine erosion. This may depend on the dimension of the estuary and sediment characteristics; in the Changjiang Delta, fine mud deposits are typically remobilized during each flood season, because of the large river discharge (Cooper, 1990; Gallagher et al., 2018).

Our study also compared morphodynamic changes during the extreme riverine discharge of 2016 to those occurring during normal high flow in the absence of typhoons (in 2011 and 2013). We found that erosion-deposition patterns in the flood season were almost the same during extreme and normal high flow, and were characterized by strong erosion (accompanied by localized siltation) in the inner estuary and weak erosion (except for strong erosion near the Jiuduansha shoal) in the offshore area (Figure 2a, 3a, S3a-S3b and S5a-S5b). In particular, elongated patches of erosion and deposition developed with a strong spatial correlation. The SHDIs of bathymetric change caused by high riverine flows were larger, and peak of cross-

sectional spectral energy were located in the inner estuary (Table S6, and Figure 2c, S2c). It should be noted that variations in Changjiang discharge in different years prompted different levels of erosion in the delta (Figure S8). For example, in 2011 and 2013 with normal riverine flow, the net erosion volumes were -54.55×10^6 m^3 and -29.79×10^6 m^3, respectively, while in 2016 the erosion increased to -64.48×10^6 m^3 due to significantly higher runoff. Therefore, flow during the flood season triggers estuarine erosion, and the larger the runoff the larger is the sediment volume scoured (Figure 4d).

4.2 Impact of TCs

TCs can transport landward re-suspended sediments and deposit them in inner estuaries, due to enhanced bottom shear stresses caused by energetic waves and storm surge currents (Warner et al., 2008; Cho et al., 2012). This landward flux of sediments can counteract the erosion induced by riverine flow during the flood season (Figure 4e, and S7d-S7e). In particular, the depocenter located offshore may move upstream, reducing the erosion in the inner estuary but increasing the erosion in offshore areas (Figure 3a and S5b). After Typhoon Ampil in 2018, large-scale erosion of more than 10 cm affected the offshore area, while alleviating the strong erosion that occurred near Jiuduansha shoal in 2016. The typhoon also triggered irregular deposition in the inner estuary, increasing size of bedforms and tidal bars (high spectral energy in the cross-sectional variations). Similar geomorphic changes were also detected in other estuaries worldwide, with TCs triggering morphodynamic processes that transform estuarine offshore areas in a short time span (Vested et al., 2013; Freeman et al.; 2015; Nowacki et al., 2015).

In recent decades, the inner SP has been weakly affected by waves during the flood season even in the presence of typhoons (Yun, 2004), tidal currents have also been stable, giving rise to a relatively steady morphology along the SP (Dai et al., 2015). Anthropogenic modifications mainly occurred several decades ago, and in recent years were minimal with little impact on its bathymetry (Wei et al., 2019). An upstream diversion project was completed in 1998 (Figure S9), and tidal flat reclamations were carried out mostly before 2014 (Figure S9g-S9h). Therefore, the morphological variations detected in 2018 can be largely attributed to Typhoon Ampil.

Bathymetric changes induced by Typhoon Kai-tak and Chan-hom in the SP show that erosion-deposition dynamics were consistent during tropical cyclones. Erosion increased in the offshore tidal flats, while decreased in the inner estuary. Therefore, geomorphologic changes generated by three typhoons all indicated that TCs cause accretion with scattered patches of deposition-erosion (Figure 3a, S5a-S5b), which can effectively alleviate the erosion produced by the river high flow, especially after the reduction of sediment load triggered by the TGD construction (Dai et al., 2018). However, some differences arose from variations in typhoons path and intensity. For instance, Typhoon Chan-hom in 2015 was strong, but its track was located far from the SP; as a result, few deposition patches over 30 cm of thickness developed upstream the mouth bars area (Figure S5b). Typhoon Ampil and Typhoon Kai-tak directly landed in Shanghai and triggered scour that extended upstream (Figure 3a and S5a). Typhoon Winnie in August 1997 eroded a large amount of offshore sediment and transported it landward (Dai et al., 2014). Between 0 and 2 TCs with similar magnitude hit the Changjiang Delta every year, affecting its morphodynamics (Table S7, Yun 2004). During these typhoons, waves eroded and deposited sediments in localized patches, resulting in more peaks in the cross-sectional spectral energy and a smaller SHDI of bottom variations with respect to the case with only river flow. The net erosion volume in the SP after the TGD construction (from 2005 to 2018) averaged around 19.4×10^6 m^3/yr. Before the dam (from 1979 to 2000), the SP was characterized by an average deposition of 13.8×10^6 m^3/yr (Table S1). The landward sediment transport triggered by one typhoon is estimated here between 17.83 and 31.22×10^6 m^3. We therefore conclude that typhoons have a long-term mitigation effect on the current erosive trend (Palinkas et al., 2014; Du et al., 2019; Wei et al., 2019). These findings also explain why estuarine tidal flats and shoals are still prograding despite the SSD of the Changjiang has dramatically decreased in recent years. Nevertheless, the vulnerability of some shorelines and channels to erosion needs to be recognized. Moreover, seaward sediment carried upstream by TCs should be efficiently intercepted and utilized to mitigate the scour triggered by sediment-depleted river discharge.

5. Conclusions

This study sheds light on the morphological variations induced by typhoons in the South Passage, Changjiang Delta, China, during the flood season. Our key conclusions are:

1. High riverine flows cause massive net erosion during flood seasons, with the removal of 29.8×10^6 m^3 of sediments in 2013 and 64.68×10^6 m^3 in 2016. High river flow scoured elongated patches parallel to the river axis in the inner estuary, while erosion was weak in the offshore area. This resulted in a higher SHDI of bathymetric change with erosion occurring at all scales.
2. Typhoons reduced the overall erosion during the flood season, with a reduction of removed volume equal to 11.96×10^6 m^3 in 2015 and 33.26×10^6 m^3 in 2018. Typhoons triggered scattered erosion and deposition without spatial structure, thus generating a lower SHDI. An increase in landward sediment transport led to localized depositional patches.
3. Typhoons effectively alleviated the erosion caused by high runoff up to 48.42 % in 2018 compared to 2016, and up to 59.86% in 2015 compared to 2013. Reduction in net erosion was more apparent in the inner estuary, while the offshore areas was characterized by mixed erosive and depositional processes.

Given the importance of storms and offshore morphodynamics on the long-term sediment budget of large deltas, we advocate that more comprehensive studies of storm effects should be undertaken worldwide, especially in the large deltas (Besset et al., 2019).

Acknowledgments

This research presented was supported by the Key Projects of Intergovernmental Science and Technology Innovation Cooperation of the Ministry of Science and Technology in China (2018YFE0109900), the International Science & Technology Cooperation Foundation Projects of Shanghai Science and Technology Commission (19230712400), the Fundamental Research Funds for the Central Universities and ECNU Academic Innovation Promotion Program for Excellent Doctoral Students (YBNLTS2019-008). Sergio Fagherazzi was partly funded by the USA National Science Foundation award 1637630 (PIE LTER), and 1832221 (VCR LTER). We are grateful to Dr. Kathleen Donohue and the anonymous reviewers for their constructive comments and suggestions that significantly improved the quality of this study. The main

statistical and analytical data involved in this study are available online (http://doi.org/10.5281/zenodo.4050566), including bathymetric change magnitudes, morphodynamic characteristics, detailed information of TCs and the monthly water-sediment discharges of the Changjiang at Datong, etc. More tropical cyclones data can be obtained from the Japan Meteorological Agency (http://www.jma.go.jp/jma/jma-eng/jma-center/rsmc-hp-pub-eg/trackarchives.html), and used Landsat remote imageries were downloaded from the U.S. Geological Survey (https://glovis.usgs.gov/app?fullscreen=0).

Supporting information

The supporting information including three paragraphs, nine figures and seven tables.

References

Allison, M. A., Weathers III, H. D., & Meselhe, E. A. (2017). Bottom morphology in the Song Hau distributary channel, Mekong River delta, Vietnam. Continental Shelf Research, 147, 51-61. https://doi.org/10.1016/j.csr.2017.05.010

Besset, M., Anthony, E. J., & Bouchette, F. (2019). Multi-decadal variations in delta shorelines and their relationship to river sediment supply: An assessment and review. *Earth Science Reviews, 193,* 199-219. https://doi.org/10.1016/j.earscirev.2019.04. 018

Castagno, W. E., Tveit, M. S., Fjellstad, W. J., & Fry, G. L. (2006). Relationships between visual landscape preferences and map-based indicators of landscape structure. *Landscape and Urban Panning, 78(4),* 465-474. https://doi.org/10.1016/ j.landurbplan.2005.12.006

Castaing, P., & Allen, G. P. (1981). Mechanisms controlling seaward escape of suspended sediment from the Gironde: a macrotidal estuary in France. *Marine Geology*, 40(1-2), 101-118. https://doi.org/10.1016/0025-3227(81)90045-1

Chen, S.L., Zhang, G.A., Yang, S.L., & Shi, J. Z. (2006). Temporal variations of fine suspended sediment concentration in the Changjiang River estuary and adjacent coastal waters, China. *Journal of Hydrology*, 331(1-2), 137-145.

Cho, K. H., Wang, H. V., Shen, J., Valle-Levinson, A., & Teng, Y. C. (2012). A modeling study on the response of Chesapeake Bay to hurricane events of Floyd and Isabel. *Ocean*

Modelling, 49, 22-46. https://doi.org/10.1016/j.ocemod.2012.02.005

Cooper, J. A. G. (2002). The role of extreme floods in estuary-coastal behaviour: Contrasts between river-and tide-dominated microtidal estuaries. *Sedimentary Geology, 150(1-2),* 123-137. https://doi.org/10.1016/S0037-0738(01)00271-8

Cooper, J. A. G., Mason, T. R., Reddering, J. S. V., & Illenberger, W. K. (1990). Geomorphological effects of catastrophic flooding on a small subtropical estuary. *Earth Surface Processes and Landforms, 15(1),* 25-41. https://doi.org/10. 1002/esp.3290150104

Dai, Z. J., Chu, A., Li, W. H., Li, J. F., & Wu, H. L. (2013). Has suspended sediment concentration near the mouth bar of the Yangtze (Changjiang) Estuary been declining in recent years? *Journal of Coastal Research, 29(4),* 809-818. https://doi.org/10. 2112/jcoastres-d-11-00200.1

Dai, Z. J., Liu, J. T., & Wen, W. (2015). Morphological evolution of the south passage in the Changjiang (Yangtze River) estuary, China. *Quaternary International*, 380, 314-326. https://doi.org/10.1016/j.quaint.2015.01.045

Dai, Z. J., Fagherazzi, S., Mei, X. F., & Gao, J. J. (2016). Decline in suspended sediment concentration delivered by the Changjiang (Yangtze) River into the East China Sea between 1956 and 2013. *Geomorphology, 268,* 123-132. https://doi.org/10.1016/j. geomorph.2016.06.009

Dai, Z. J., Liu, J. T., Wei, W., & Chen, J. Y. (2014). Detection of the Three Gorges Dam influence on the Changjiang (Yangtze River) submerged delta. *Scientific Reports, 4(6600),* 1-7. https://doi.org/10.1038/srep06600

Dai, Z. J., Mei, X. F., Darby, S. E., Lou, Y. Y, & Li, W. H. (2018). Fluvial sediment transfer in the Changjiang (Yangtze) river-estuary depositional system. *Journal of hydrology, 566,* 719-734. https://doi.org/10.1016/j.jhydrol.2018.09.019

Du, J. B., Park, K., Dellapenna, T. M., & Clay, J. M. (2019). Dramatic hydrodynamic and sedimentary responses in Galveston Bay and adjacent inner shelf to Hurricane Harvey. *Science of the Total Environment, 653,* 554-564. https://doi.org/10.1016/j. scitotenv.2018.10.403

Fagherazzi, S., & Overeem, I. (2007). Models of deltaic and inner continental shelf landform evolution. Annu. Rev. Earth Planet. Sci., 35, 685-715. https://doi.org/

10.1146/annurev.earth.35.031306.140128

Filgueira, R., Guyondet, T., Comeau, L. A., & Grant, J. (2014). Storm-induced changes in coastal geomorphology control estuarine secondary productivity. *Earth's Future, 2(1),* 1-6. https://doi.org/10.1002/2013EF000145

Freeman, A. M., Jose, F., Roberts, H. H., & Stone, G. W. (2015). Storm induced hydrodynamics and sediment transport in a coastal Louisiana lake. *Estuarine, Coastal and Shelf Science, 161,* 65-75. https://doi.org/10.1016/j.ecss.2015.04.011

Gallagher, J. B., & Ross, D. J. (2018). Sediment geochronology for bar-built estuaries subject to flood deposition and erosion: A robust multiproxy approach across an estuarine zone. *The Holocene*, *28(3),* 341-353. https://doi.org/10.1177/09596836177 29441

Gracia, A., Rangel-Buitrago, N., Oakley, J. A., & Williams, A. T. (2018). Use of ecosystems in coastal erosion management. *Ocean & coastal management, 156,* 277-289. https://doi.org/10.1016/j.ocecoaman.2017.07.009

Hu, K., Ding, P., Wang, Z., & Yang, S. (2009). A 2D/3D hydrodynamic and sediment transport model for the Yangtze Estuary, China. *Journal of Marine Systems, 77(1-2),* 114-136. https://doi.org/10.1016/j.jmarsys.2008.11.014

Kroon, A., Larson, M., Möller, I., Yokoki, H., Rozynski, G., Cox, J., & Larroude, P. (2008). Statistical analysis of coastal morphological data sets over seasonal to decadal time scales. *Coastal Engineering, 55(7-8)*, 581-600. https://doi.org/10.1016/ j.coastaleng.2007.11.006

Lentz, E. E., & Hapke, C. J. (2011). Geologic framework influences on the geomorphology of an anthropogenically modified barrier island: assessment of dune/beach changes at Fire Island, New York. *Geomorpholog*y, 126(1-2), 82-96. https://doi.org/10.1016/j.geomorph. 2010.10.032

Lesourd, S., Lesueur, P., Brun-Cottan, J. C., Garnaud, S., & Poupinet, N. (2003). Seasonal variations in the characteristics of superficial sediments in a macrotidal estuary (the Seine inlet, France). *Estuarine, Coastal and Shelf Science*, *58(1),* 3-16. https://doi.org/10.1016/S0272-7714(02)00340-2

Masselink, G., Castelle, B., Scott, T., Dodet, G., Suanez, S., Jackson, D., & Floc'h, F. (2016). Extreme wave activity during 2013/2014 winter and morphological impacts along the Atlantic coast of Europe. *Geophysical Research Letters, 43(5),* 2135-2143.

https://doi.org/10.1002/2015GL067492

Mei, X.F., Dai, Z.J., Wei, W., Li, W.H., Wang, J., & Sheng, H. (2018). Secular bathymetric variations of the North Channel in the Changjiang (Yangtze) Estuary, China, 1880–2013: Causes and effects. *Geomorphology, 303,* 30-40. https://doi.org/ 10.1016/j.geomorph.2017.11.014

Miles, T., Seroka, G., Kohut, J., Schofield, O., & Glenn, S. (2015). Glider observations and modeling of sediment transport in Hurricane Sandy. *Journal of Geophysical Research: Oceans, 120(3),* 1771-1791. https://doi.org/10.1002/2014JC010474

Miselis, J. L., Andrews, B. D., Nicholson, R. S., Defne, Z., Ganju, N. K., & Navoy, A. (2016). Evolution of mid-Atlantic coastal and back-barrier estuary environments in response to a hurricane: Implications for barrier-estuary connectivity. Estuaries and Coasts, 39(4), 916-934. https://doi.org/10.1007/s12237-015-0057-x

Miner, M. D., Kulp, M. A., FitzGerald, D. M., & Georgiou, I. Y. (2009). Hurricane-associated ebb-tidal delta sediment dynamics. *Geology, 37(9),* 851-854. https://doi. org/10.1130/G25466A.1

Nowacki, D. J., Ogston, A. S., Nittrouer, C. A., Fricke, A. T., & Van, P. D. T. (2015). Sediment dynamics in the lower M ekong R iver: Transition from tidal river to estuary. *Journal of Geophysical Research: Oceans, 120(9),* 6363-6383. https://doi.org/10.1002/2015JC010754

Ortiz, A. C., Roy, S., & Edmonds, D. A. (2017). Land loss by pond expansion on the Mississippi River Delta Plain. *Geophysical Research Letters, 44(8),* 3635-3642. https://doi.org/10.1002/2017GL073079

Palinkas, C. M., Halka, J. P., Li, M., Sanford, L. P., & Cheng, P. (2014). Sediment deposition from tropical storms in the upper Chesapeake Bay: field observations and model simulations. *Continental Shelf Research, 86,* 6-16. https://doi.org/10.1016/ j.csr.2013.09.012

Sibson, R. (1981). A Brief Description of Natural Neighbor Interpolation. Interpreting Multivariate Data, John Wiley & Sons, New York, 21-36.

Syvitski, J. P., Vörösmarty, C. J., Kettner, A. J., & Green, P. (2005). Impact of humans on the flux of terrestrial sediment to the global coastal ocean. *Science, 308(5720),* 376-380. https://doi.org/10.1126/science.1109454

Tramer, E. J. (1969). Bird species diversity: components of Shannon's formula. Ecology, 50(5),

927-929. https://doi.org/10.2307/1933715

Van Maren, D. S., & Hoekstra, P. (2004). Seasonal variation of hydrodynamics and sediment dynamics in a shallow subtropical estuary: the Ba Lat River, Vietnam. Estuarine, *Coastal and Shelf Science, 60(3),* 529-540. https://doi.org/10.1016/j.ecss. 2004.02.011

Vested, H. J., Tessier, C., Christensen, B. B., & Goubert, E. (2013). Numerical modelling of morphodynamics-Vilaine Estuary. *Ocean Dynamics, 63(4)*, 423-446. https://doi.org/10.1007/s10236-013-0603-7

Wan, Y. Y., Roelvink, D., Li, W. H., Qi, D. M., & Gu, F. F. (2014). Observation and modeling of the storm-induced fluid mud dynamics in a muddy-estuarine navigational channel. *Geomorphology, 217,* 23-36. https://doi.org/10.1016/j.geom orph.2014.03.050

Wang, J., Dai, Z. J., Mei, X. F., Lou, Y. Y., Wei, W., & Ge, Z. P. (2018). Immediately downstream effects of Three Gorges Dam on channel sandbars morphodynamics between Yichang-Chenglingji Reach of the Changjiang River, China. *Journal of Geographical Sciences, 28(5),* 629-646. https://doi.org/10.1007/s11442-018-1495-8

Warner, J. C., Butman, B., & Dalyander, P. S. (2008). Storm-driven sediment transport in Massachusetts Bay. *Continental Shelf Research, 28(2),* 257-282. https://doi.org/10. 1016/j.csr.2007.08.008

Wei, W., Dai, Z. J., Mei, X. F., Liu, J. P., Gao, S., & Li, S. S. (2017). Shoal morphodynamics of the Changjiang (Yangtze) estuary: Influences from river damming, estuarine hydraulic engineering and reclamation projects. *Marine Geology*, 386, 32-43. https://doi.org/10.1016/j.margeo.2017.02.013

Wei, W., Dai, Z., Mei, X., Gao, S., & Liu, J. P. (2019). Multi-decadal morpho-sedimentary dynamics of the largest Changjiang estuarine marginal shoal: Causes and implications. *Land Degradation & Development*, 30(17), 2048-2063.

Woodroffe, C. D., Chappell, J., Thom, B. G., & Wallensky, E. (1989). Depositional model of a macrotidal estuary and floodplain, South Alligator River, Northern Australia. *Sedimentology, 36(5),* 737-756. https://doi.org/10.1111/j.1365-3091.1989. tb01743.x

Yang, H. F., Yang, S. L., Xu, K. H., Wu, H., Shi, B. W., Zhu, Q., Yang, Z. (2017). Erosion potential of the Yangtze Delta under sediment starvation and climate change. *Scientific reports, 7(1),* 10535. https://doi.org/10.1038/s41598-017-10958-y

Yang, S. L., Friedrichs, C. T., Shi, Z., Ding, P. X., Zhu, J., & Zhao, Q. Y. (2003). Morphological response of tidal marshes, flats and channels of the outer Yangtze River mouth to a major storm. *Estuaries, 26(6),* 1416-1425. https://doi.org/10.1007/ BF02803650

Yun, C. X. (2004). Basic Law of the Recent Evolution of the Changjiang Estuary. Beijing, China Ocean Press.

Zhang, X. H., Fagherazzi, S., Leonardi, N., & Li, J. F. (2018). A positive feedback between sediment deposition and tidal prism may affect the morphodynamic evolution of tidal deltas. *Journal of Geophysical Research: Earth Surface, 123(11),* 2767-2783. https://doi.org/10.1029/2018JF004639

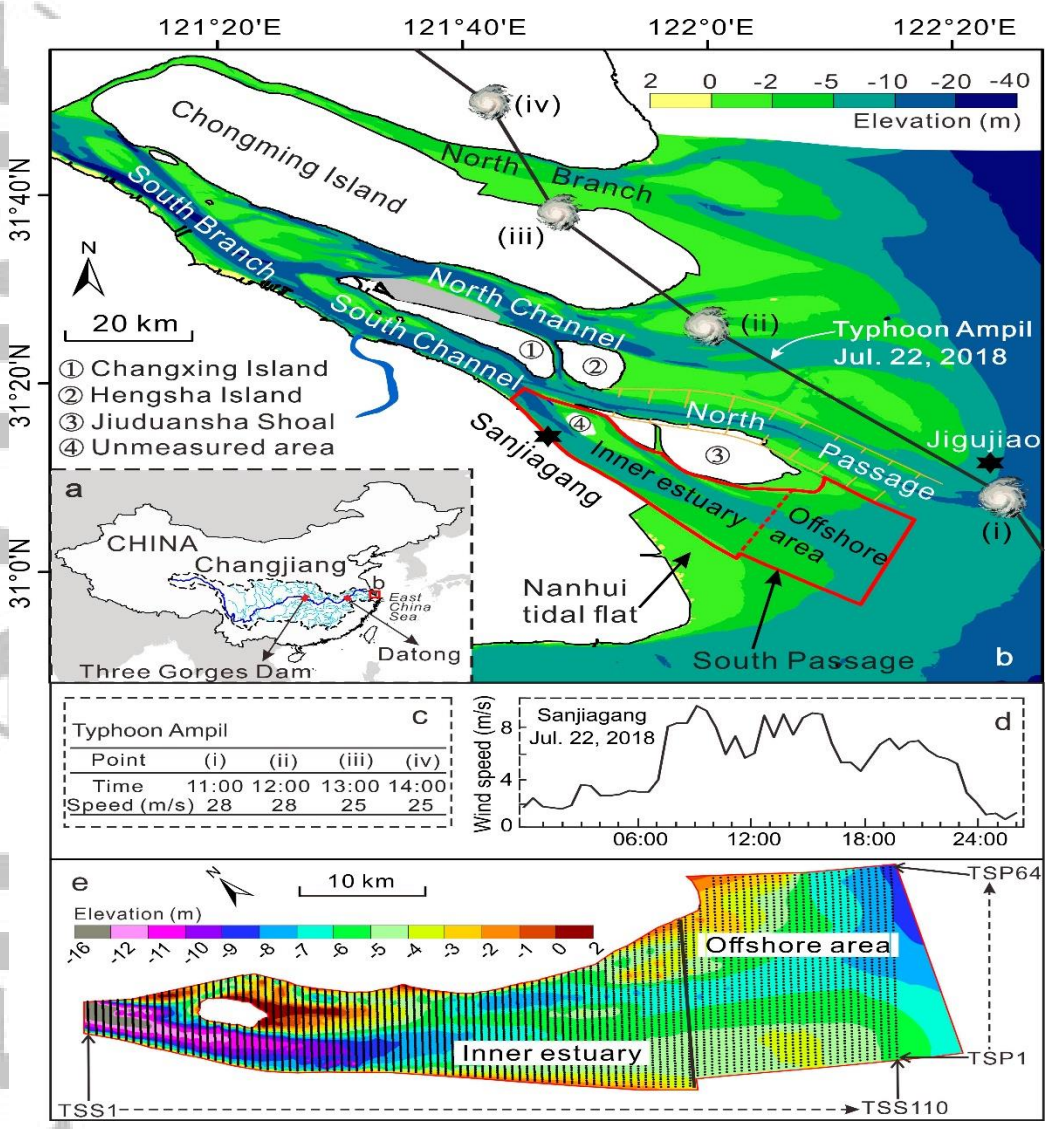

Figure 1. Study area. (a) Location of the Changjiang River in China; the Datong hydrological station is located at the tidal limit. (b) Bathymetric map of the Changjiang Delta in 2011, the black solid line and corresponding nodes represents the pathway of Typhoon Ampil on 22 July 2018; the red polygon is the South Passage (SP), divided into inner estuary and offshore area. (c) Timing and wind speed of Typhoon Ampil passage across the Changjiang Delta. (d) Wind speed on 22 July 2018 measured at Sanjiagang meteorological station. (e) 110 transverse sampling section (TSS) along the SP used for the calculation of 1D Fast Fourier Transform, the 64 transverse sampling points (TSP) are evenly spaced along each transverse section. The background is the bathymetric map of June 2018.

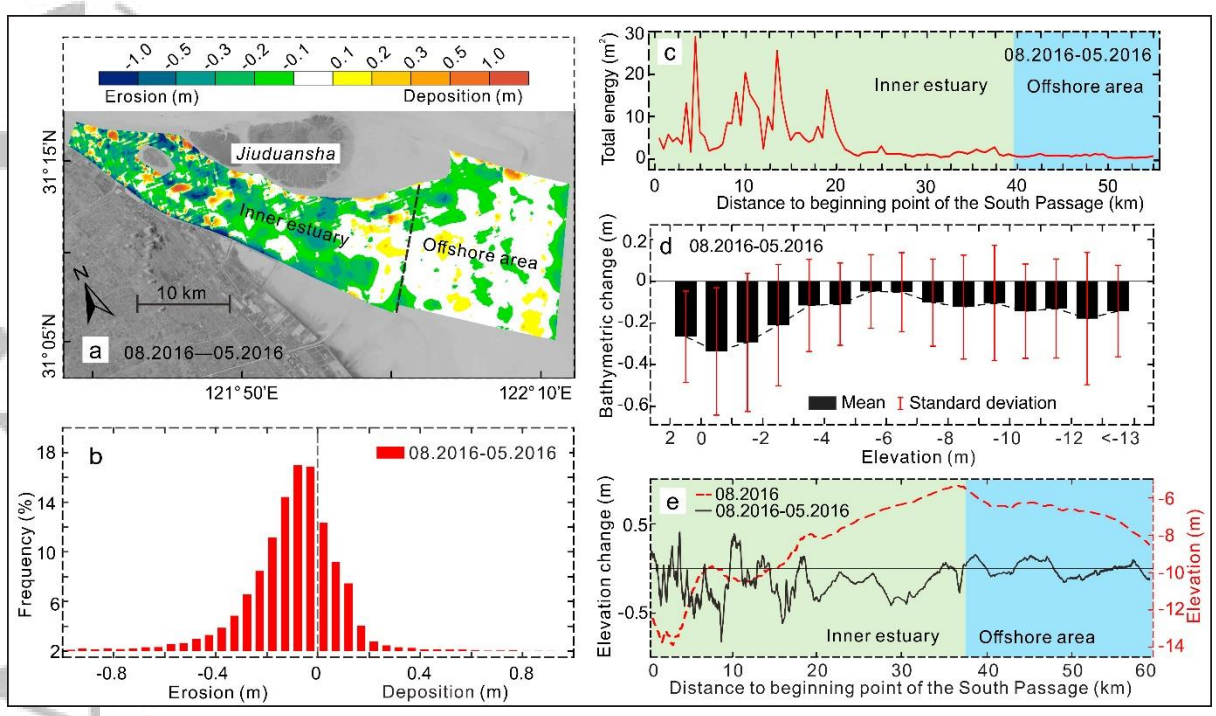

Figure 2. Bathymetric changes in the SP induced by high riverine flow in the flood season from May to August 2016. (a) Erosion and deposition patterns in the inner estuary and offshore area. (b) Frequency histogram of erosion and deposition magnitudes. (c) Longitudinal variation of the total spectral energy computed at the 110 transverse sampling sections of Figure 1e. (d) Mean bathymetric change in each elevation interval. (e) Changes of thalweg elevation (black solid line) with respect to the original thalweg in August 2016 (red dashed line).

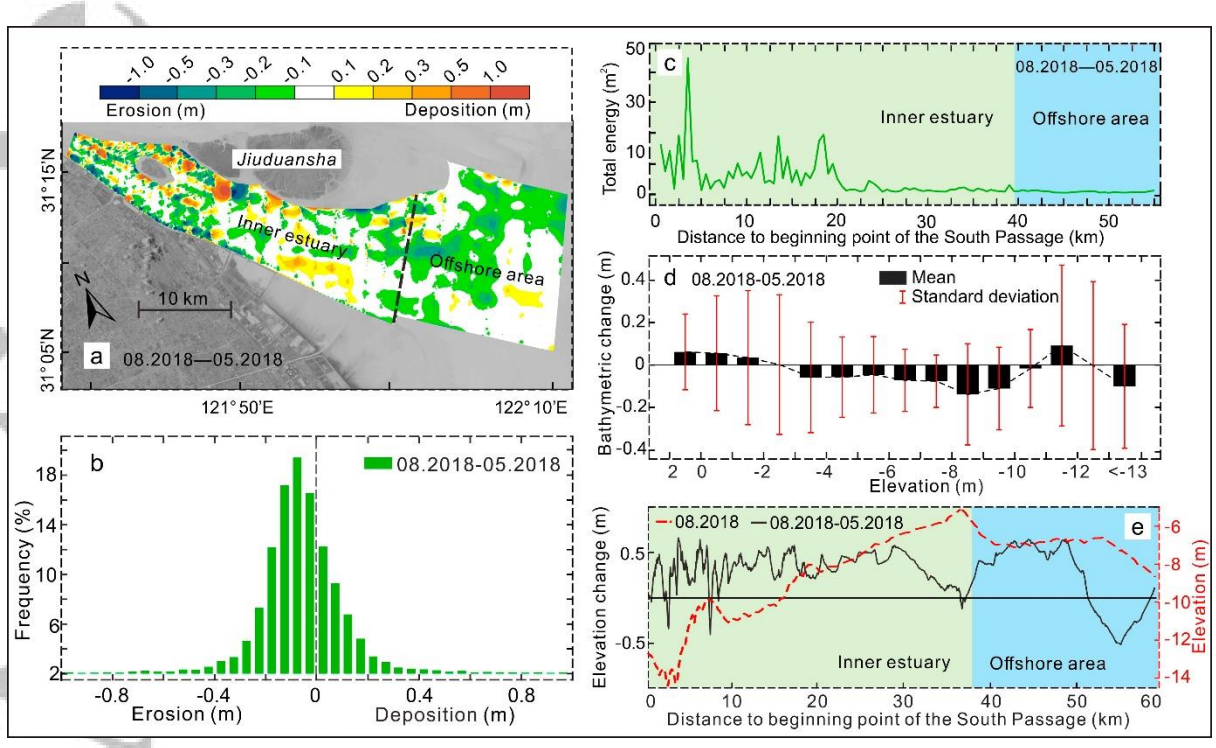

Figure 3. Bathymetric changes triggered by Typhoon Ampil in July 2018 along the SP. (a) Erosion and deposition patterns in the inner estuary and offshore area from May to August. (b) Frequency histogram of erosion and deposition magnitudes induced by Ampil. (c) Longitudinal variation of total spectral energy computed along the 10 transverse sampling sections of Figure 1e. (d) Mean bathymetric change in each elevation interval. (e) Changes of thalweg elevation (black solid line) with respect to the original thalweg elevations in Aug. 2018 (red dashed line).

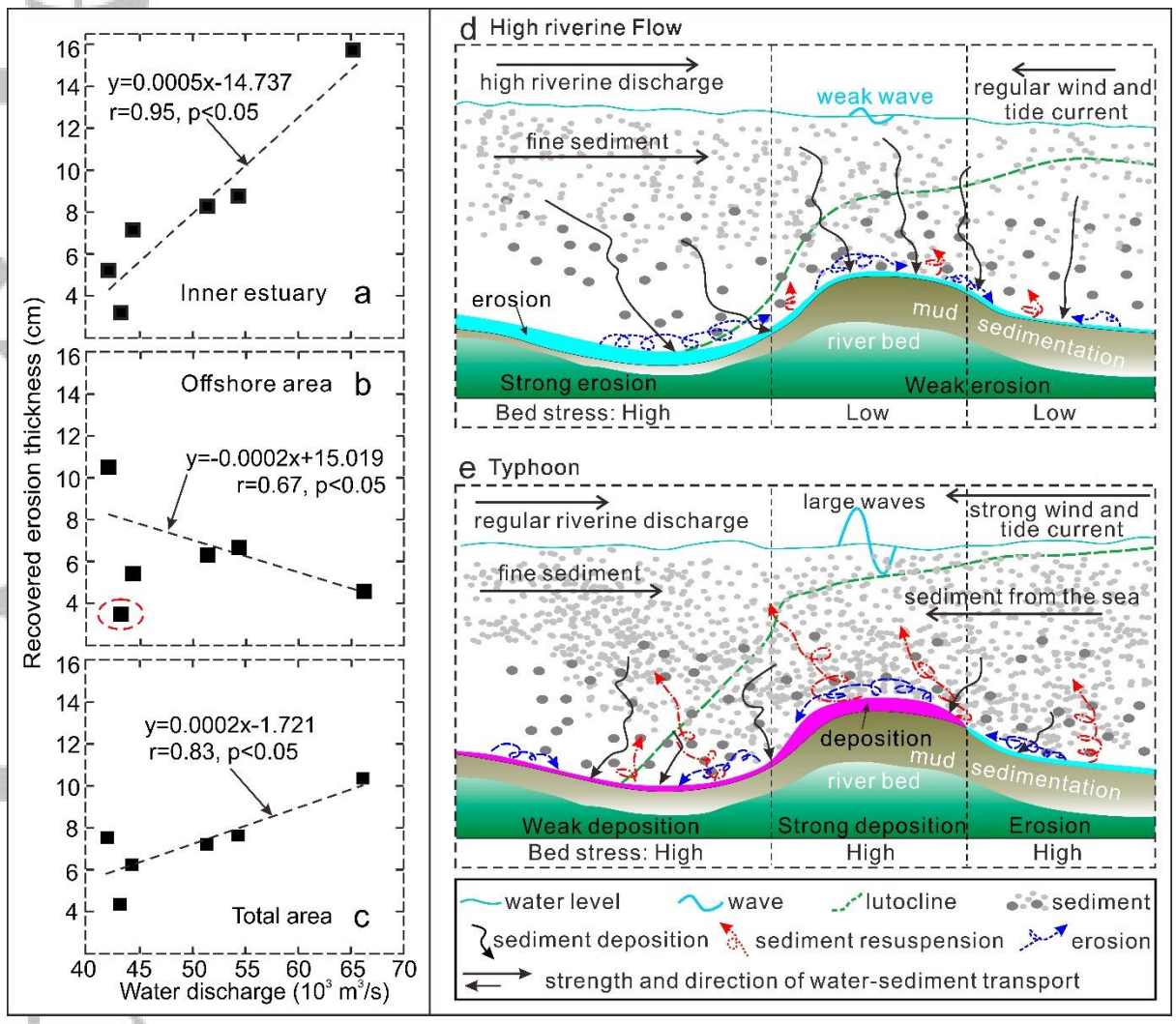

Figure 4. Relationship between annual recovered erosion thickness and average value of the top 30 river water discharges in each year: (a) inner estuary, (b) offshore area (value in red ellipse was excluded) and (c) entire SP. Conceptual model showing the hydrodynamics, sediment dynamics and bathymetric changes in the inner estuary and offshore area induced by (d) high riverine flow and (e) a typhoon.